Development of CO_2 Laser Produced Xe Plasma EUV Light Source for Microlithography

Hakaru Mizoguchi*, Akira Endo, Tatsuya Ariga, Taisuke Miura, Hideo Hoshino, Yoshifumi Ueno, Masaki Nakano, Hiroshi Komori, Akira Sumitani, Tamotsu Abe, Takashi Suganuma, Georg Soumagne, Hiroshi Someya,Yuichi Takabayashi, Koichi Toyoda
Hiratsuka Research & Development Center, EUVA
(Extreme Ultraviolet Lithography System Development Association),
1200 Manda, Hiratsuka-shi, Kanagawa, 254-8567, Japan
phone +81-463-35-9351 ; fax +81-463-35-9352;
http://www.euva.or.jp

ABSTRACT

A CO_2 laser driven Xe droplet plasma is presented as a light source for EUV lithography. A short-pulse TEA CO_2 master oscillator power amplifier system and a pre-pulse Nd:YAG laser were used for initial experiment with 0.6% of CE from a Xe jet. A target technology is developed for high average power experiments based on a Xe droplet at 100kHz. Magnetic field ion mitigation is shown to work well in the pre-pulsed plasma combined with a CO_2 laser main pulse. This result is very promising with respect to collector mirror lifetime extension by magnetic field mitigation. A master oscillator power amplifier (MOPA) CO_2 laser system is under development with a few kW and 100 kHz repetition rate with less than 15ns laser pulse width using a waveguide Q-switched CO_2 laser oscillator and RF-excited fast axial flow CO_2 laser amplifiers.

Keywords: EUV light source, laser-produced plasma, CO_2 Laser, Xe plasma, droplet, magnetic field

1. INTRODUCTION

The main technical challenge of a laser produced plasma (LPP) EUV light source for microlithography is to realize a EUV power of 115W at the intermediate focus[1]. Based on the research we performed since the establishment of EUVA in 2002, we have concluded that the 100 W level EUV cannot be obtained based on solid-state Nd:YAG driver laser technology, which is currently limited to kW laser power level. This approach will require multiplexing of too many laser modules, which will make the system layout too complex and too expensive[2]. Instead, CO_2 laser technology will be used that can produce 10 kW level average output powers[3]. Based on this technology, we have selected the following LPP EUV source system that is composed of a CO_2 driver laser, Xe droplet target supply and magnetic field ion mitigation. This source system is expected to realize a HVM in the next generation. A short pulse width CO_2 laser has been chosen to produce EUV emission effectively with a pre-irradiation. CE (2%bw, 2πsr) of 0.6% has been achieved with a 25 ns pulse width CO_2 laser with a pre-pulse YAG laser of 8ns in low repetition rate operation. Based on this experimental result, a laser system with less than 15ns laser pulse width, master oscillator power amplifier (MOPA) CO_2 laser system of a few kW and 100 kHz repetition rate is under development using a waveguide Q-switched CO_2 laser and RF-excited fast axial flow CO_2 laser amplifiers. We are constructing this system in the beginning of 2006, and use it as a driver laser for 10W EUV power at the intermediate focus. A Xe droplet target has been chosen as a target which is suitable for high repetition rate target supply with uniform shape in high speed. The droplets are made by continuous jet method and a piezoelectric element (PZT) attached to a nozzle, induces a Rayleigh instability that causes the jet to break up into droplets. Applying the appropriate nozzle oscillation frequency for a given droplet speed and nozzle diameter, uniform and equidistant droplets are generated. The Xe droplet speed and repetition rate we have achieved are 100 m/s and 1MHz, respectively. And the droplet supply is synchronized with our 100 kHz CO_2 laser system. We are planning to increase further the droplet speed for a high power source. A magnetic field ion mitigation to reduce damage of the collector mirror shows considerable extension of mirror lifetime. As a first step, ion mitigation with a magnetic field of 0.6T showed that the estimated lifetime was increased at 10 to 30 times. We are optimizing the magnetic field shape and strength and evaluation of the Mo/Si mirror lifetime by the optimized mitigation is reported.

2. CHARACTERRISTICS OF CO2 LASER PRODUCED Xe PLASMA

2.1. Experimental setup and CE measurement

The experimental set-up of the pre-pulsed CO_2 laser plasma characterization is shown in Fig. 1. A 3-stage TEA CO_2 :master oscillator power amplifier (MOPA) system has been developed as a driver laser for this experiment. The lasers are based on 2-kHz and 4-kHz microlithography excimer lasers from Gigaphoton Inc. Electrode shapes and laser optics were optimized for TEA CO_2 laser. The maximum repetition rate of the system was 2 kHz with output laser energy of 300 mJ in 25-ns pulse width. A pre-pulse Nd:YAG laser pulse with an output energy of 5 mJ, 8-ns pulse duration irradiated the 30-μm diameter Xe jet target prior to the main CO_2 laser pulse[4]. Figure 1 shows the experimental setup including the Xe continuous jet, pre-pulse Nd:YAG, main pulse CO_2 laser, plasma imaging Mo/Si mirror, and various diagnostics.

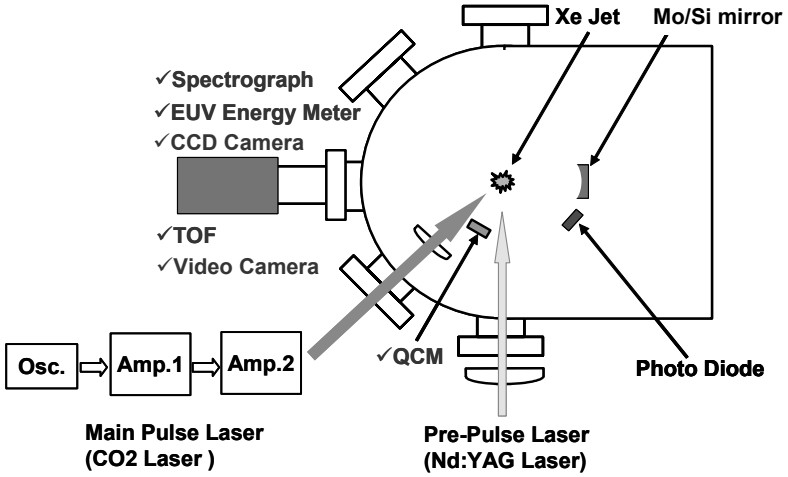

Fig. 1 Experimental setup for the pre-pulsed CO_2 laser plasma characterization

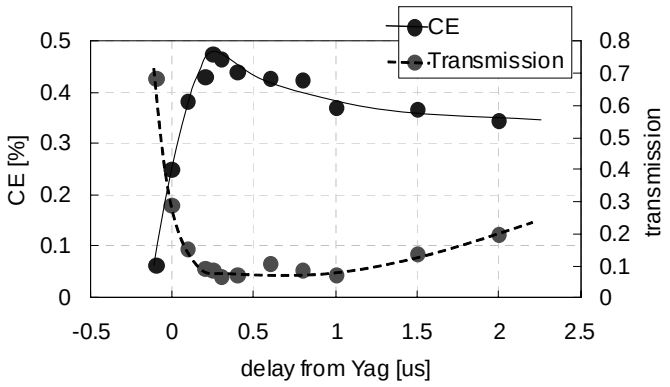

Fig. 2 CE and the CO_2 laser transmittance dependence on the delay time

The conversion efficiency from input laser energy to emitted EUV energy (2% bandwidth, 2π sr) and the transmitted CO_2 laser energy were measured at different delay times between the pre-pulse and the main pulse laser irradiation. Figure 2 shows the measured CE and the CO_2 laser transmittance versus the delay time. The input CO_2 laser energy was 75 mJ and the transmittance was measured by focusing the transmitted laser beam onto a photon drag detector with a lens. Negative delay times in the plot denote data without pre-pulse laser irradiation. A significant increase in CE and a decrease in CO_2 laser transmittance were observed using pre-pulse laser irradiation. The maximum CE of about 0.5% was obtained at the delay time of about 200 ns. The EUV output energy was measured at different CO_2 laser energies and pulse durations of 15, 25 and 45 ns with and without pre-pulse laser irradiation. The maximum CE increased two to three times with pre-pulse laser irradiation. The CE increased with increasing main pulse laser intensity. The maximum CE of 0.6% was obtained with a main pulse laser intensity of about 5.2×10^{10} W/cm^2.

2.3. Plasma image

The EUV Image of the plasma was monitored to evaluate the plasma size. A Mo/Si multilayer-coated concave mirror with radius of curvature of 500 mm was placed at 290mm from the plasma to image the plasma on a CCD camera with a magnification of 6.3. The configuration of the setup is shown in Fig. 3 (a). The CO_2 laser pulse energy was 50 mJ. Figure 3 shows the plasma image (b) pre-pulse Nd:YAG laser of 5 mJ, 8-ns, intensity of 8 x 10^9 W/cm^2 irradiation only, (c) CO_2 laser of 50 mJ, 25-ns, intensity of 6 x 10^9 W/cm^2 irradiation only. The EUV plasma image with pre-pulsed laser at different delay time from 0 ns to 1000 ns are shown in Fig. 3(d). Crescent-shaped plasma images were observed since the plasma was observed from the lateral direction of the incident laser. The monitored plasma size in the vertical direction at a delay time of 200 ns that produced the maximum EUV output was about 400 μm. The calculated etendue was 0.8 mm^{2}sr if we assume plasma size of 400 μm in diameter and collecting solid angle of 2 π sr. This etendue is within the required maximum etendue of 3.3 mm^{2}sr.[1]

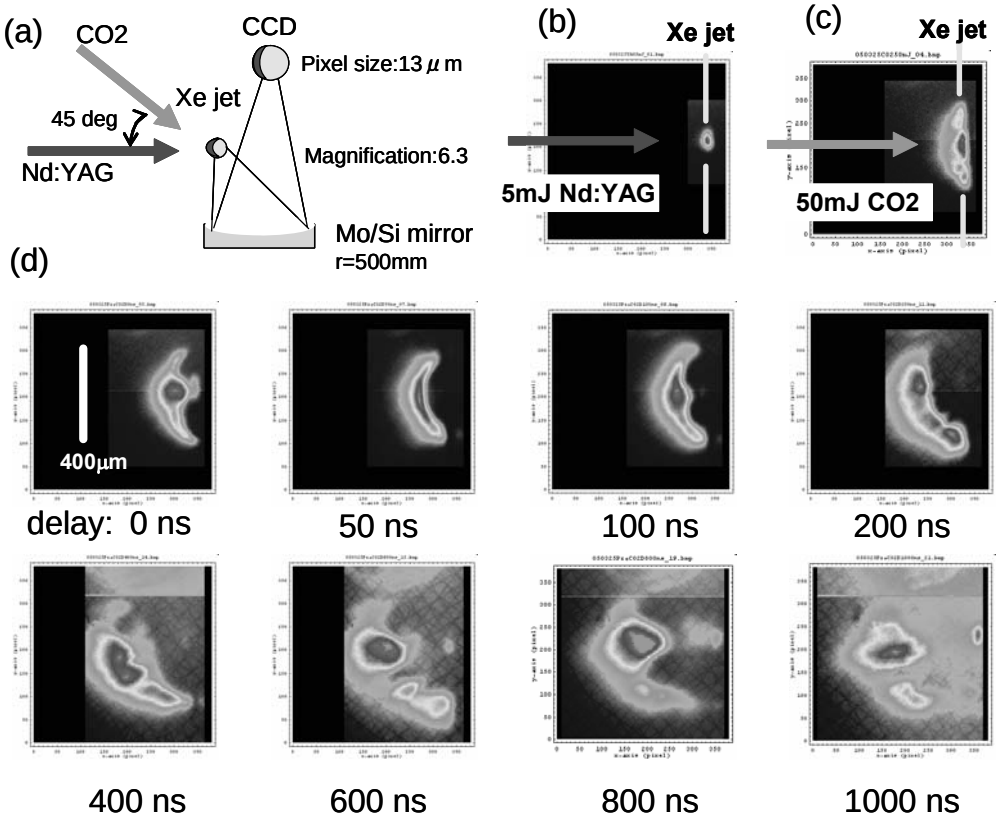

Fig.3. EUV plasma image monitored by a Mo/Si multilayer concaved mirror and a CCD camera.

2.4. Out-of-band spectra

Spectra of the plasma emission were measured at the EUV in-band and out-of-band region. The EUV in-band spectrum was monitored by a flat-field grazing incidence spectrometer using a variable-line-spacing grating (1200 grooves/mm). The measured EUV spectra were at a delay time between the pre-pulse and the main laser pulse of 0, 50, 200 and 600 ns. The maximum EUV emission spectrum was observed at a delay time of 200 ns. The peak intensity at 11 nm was relatively weak compared with a Nd:YAG laser produced plasma. This is a characteristic spectrum from a low-density plasma and it resembles a spectrum from a DPP light source and from an Nd:YAG laser produced plasma using a Xe gas puff target. The out-of-band spectra in the ultra-violet, visible and infrared region were monitored. The overall spectral profile decreased gradually with increasing wavelength. The out-of-band energy distribution was also measured by using colored glass filters and a photodiode (IRD, AXUV 100G). The dependence of the out-of-band energy distribution on the delay time is shown in Fig. 4. The out-of-band emission increased with increasing delay time between pre-pulse and main pulse laser irradiation though the EUV emission had a peak at delay time of 200 ns. The same result was obtained by integrating the out-of-band spectra measured at different delay times using a compact spectrometer.

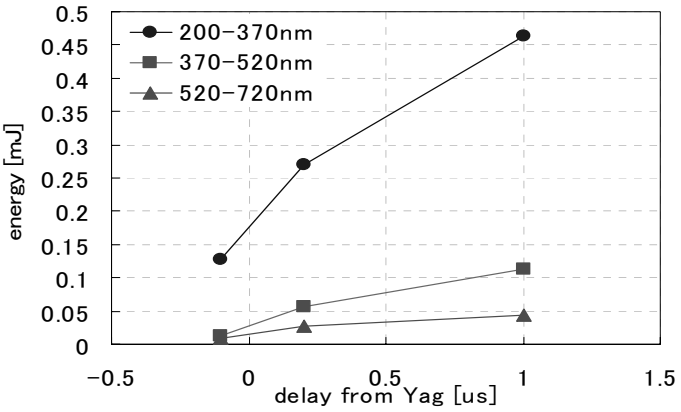

Fig.4 Out-of-band energy distribution dependence on delay time

3. XENON DROPLETS

3.1 Xenon Droplets Generation

A mass-limited target minimizes the amount of target material to be supplied. It also increases the conversion efficiency and decreases debris formation. Uniform droplet generation for high power CO2 driver laser was investigated[5]. Figure.5 shows a schematic of the Xe droplet generation and laser irradiation system. The liquefied xenon jet is ejected from the nozzle into the low vacuum chamber. The pressure inside this chamber, where the droplets form, i.e. the chamber containing the nozzle, is adjusted slightly below the triple point pressure of xenon using a buffer gas, like helium or nitrogen between 10 and 20 kPa. This avoids the xenon jet boils and freezes. The periodic oscillation of the piezoelectric transducer induces a jet surface instability causing the liquid jet to break up into uniform droplets according to the Rayleigh instability[6] . The low vacuum chamber is placed inside the main chamber and separated from it with a skimmer in order to apply differential pumping. The pressure thus obtained in the main chamber was about <1Pa during xenon droplet injection. Xenon droplets are injected into the high vacuum area through the skimmer, and irradiated by the laser beam.

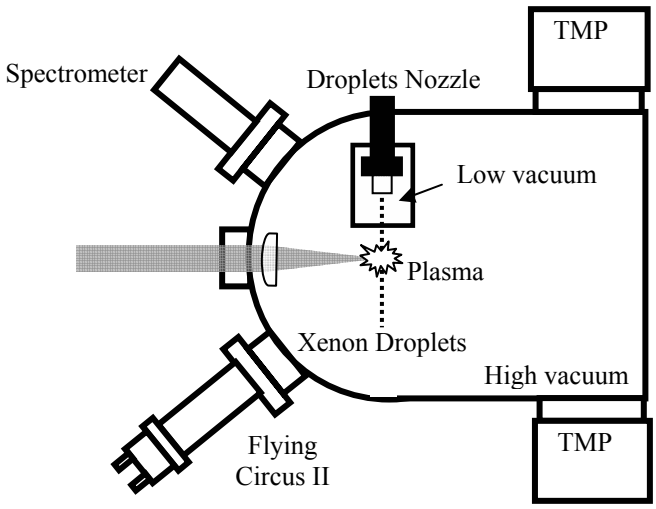

Fig.5. Schematic of the droplet generation and laser irradiation system

Figure 6 shows the relationship between λ/d and the minimum transducer amplitude in order to form uniform droplets, where λ is the wavelength of the disturbance, and d is the jet diameter. Pictures on the figure show the observed Xe droplets for each λ/d. Uniform droplets, i.e. having identical size and being equidistant, are generated for a parameter λ/d between 3 and 8 at constant transducer amplitude. Outside this range, i.e. for λ/d below 3 and above 8, the transducer amplitude required for uniform droplet generation increases significantly. For λ/d>8 small additional droplets (satellites) appear beside the main droplets, and for λ/d<3 non-uniform droplets are generated due to spontaneous disturbances.

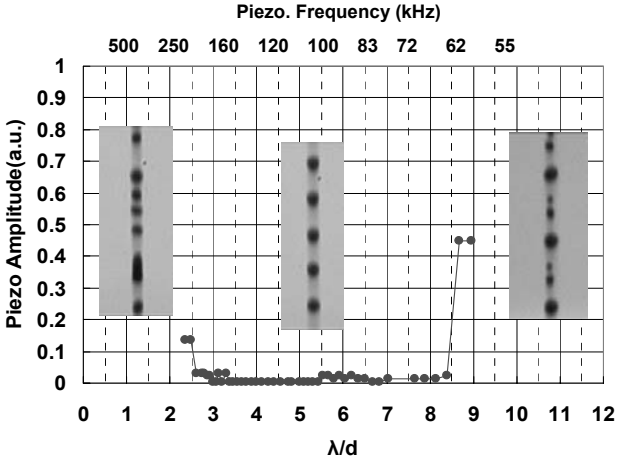

Fig.6 Relationship between piezo amplitude and λ/d for uniform droplets generation

The behavior of the laser irradiated droplets is useful information to optimize the droplet speed. Figure 7 shows the plasma and droplet behavior at 0 (left picture) and 10 μ sec (right picture) time delay. 10 μ sec corresponds to 100kHzlaser repetition rate. The right picture shows that the droplet closest to the irradiated droplet is blown away by the plasma generation, and the second droplet is slightly dislocated. This means that the next laser irradiation is to be on the third droplet. The flow speed of the droplet train is 20m/sand the distance is 200 μ m in this experiment. The optimum speed of the droplet train is thus 60m/s.

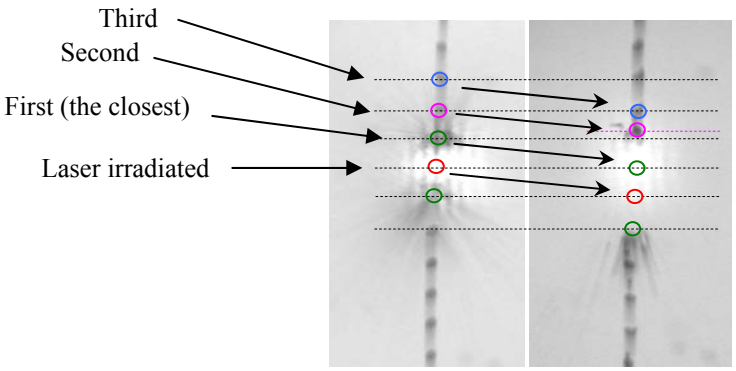

Fig.7 Droplets behavior under laser irradiation (Left: 0 delay, Right:10 μ sec delay)

3.2 High Speed Xe Droplets

The flow speed of the Xe droplet is determined by the back pressure. Figure 8 shows the relationship between the pressure and the flow speed. It is clear that more than 5MPa is required to achieve 60m/s. We have installed a compressor in the Xe control system with maximum available pressure up to 70MPa. Figure.9 shows a 100m/s droplet train generated in high vacuum <1Pa, from a 15MPa pressure droplet generator.. The droplet diameter is 60 μ m, and the frequency is 900kHz.

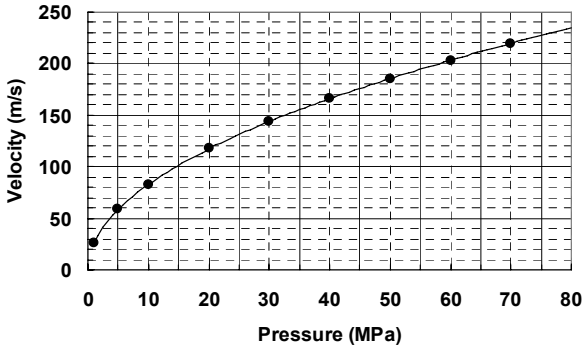

Fig.8 Xenon droplets velocity vs. pressure

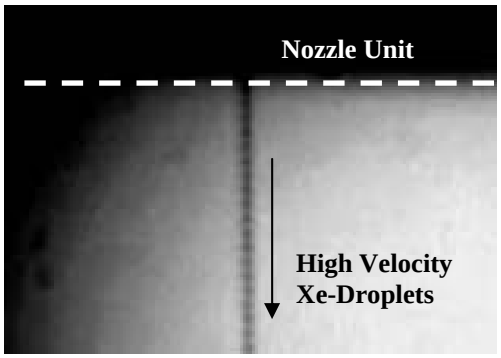

Fig.9. High velocity Xe droplets in high vacuum

4. MAGNETIC FIELD ION MITIGATION

4.1 Fast ion characteristics and mitigation

Fast ions are produced from the laser plasma together with EUV and out-of-band radiation. These fast ions significantly damage the multilayer of the collector mirror placed near the laser-plasma source. We have been characterizing fast ions and developing fast ion mitigation technology using a magnetic field confinement.[7] Fast ion characteristics may be changed from low-density plasma produced by a pre-pulse laser irradiation. We measured energy distribution and effectiveness of magnetic field mitigation for pre-pulsed CO_2 laser driven plasma.

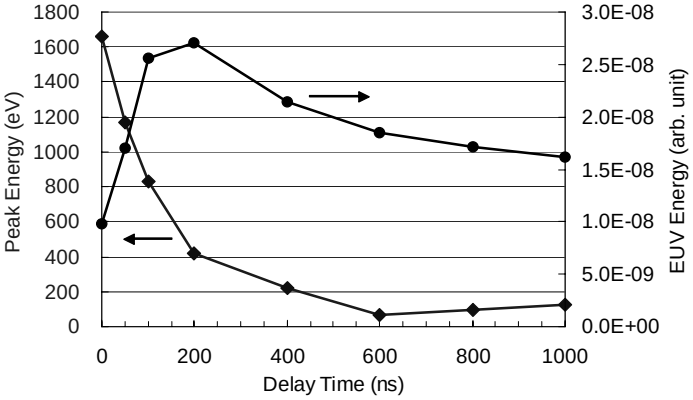

Fig.10. Peak ion energy distribution dependence on delay time

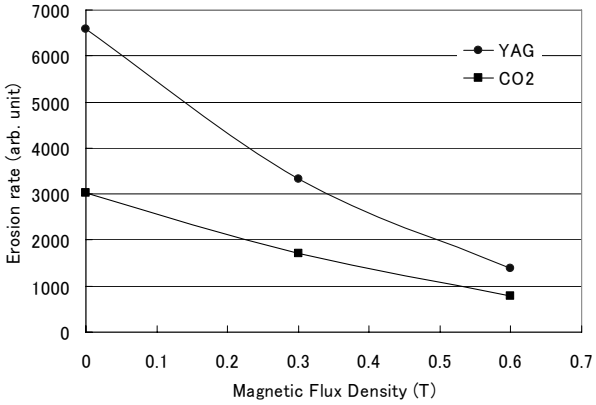

Fig.11. Erosion rate dependence on magnetic flux density

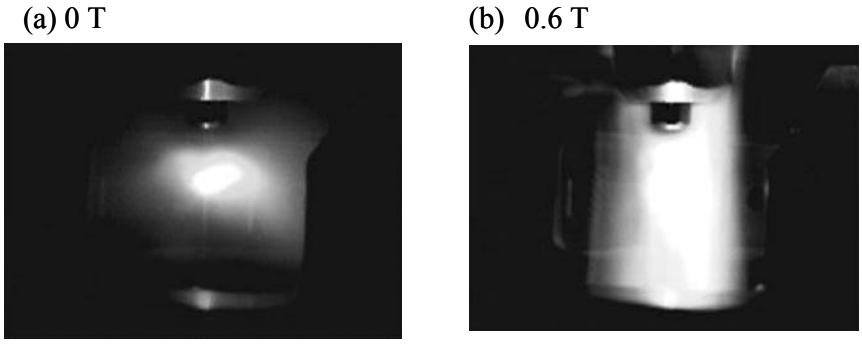

Fig.12. CO_2 laser produced plasma source image in a visible range (a) without and (b) with 0.6-T magnetic field.

Fast ion energy distributions at different delay times were measured by the TOF method. The peak energy of the ion energy distribution was observed at about 400 eV with only 5-mJ pre-pulse Nd:YAG irradiation. An additional ion energy peak at 2 keV was observed by CO_2 laser irradiation at a delay time of 0 ns. It can be seen that the peak energy of the ion energy distribution by CO_2 laser irradiation decreases with increasing delay time. Figure 10 shows the dependence of the peak energy of the ion energy distribution for CO_2 laser irradiation on delay time. The fast ion energy distribution drastically decreased after a delay time of 200 ns. This result is promising with respect to the collector mirror lifetime extension since the maximum EUV emission was obtained at a delay time of 200 ns.
A QCM was placed at about 100 mm from the plasma source and at an angle of 60 degree to the incident laser beam to monitor the effectiveness of the magnetic field ion mitigation for a pre-pulse CO_2 laser produced plasma. The quartz crystal surface of the QCM was coated with gold as sample material. The observed erosion rate of the pre-pulse CO_2 laser produced plasma was lower than that of the Nd:YAG laser produced plasma shown in Fig.11. This is due to the low-density target plasma produced by a pre-pulse irradiation.
Figure 12 shows the visible CO_2 laser produced plasma emission taken by a CCD camera at an angle of 90 degree to the laser beam axis (a) without and (b) with a magnetic flux density of 0.6 T. When the magnetic field was applied, bright plasma emission was observed like a positive column due to increased collisions between the magnetically confined particles.

5. HIGH POWER AND SHORT PULSE RF-EXCITED CO_2 LASER

5.1 Concept of the CO2 laser amplifier system

CO_2 laser chain is composed of four laser modules, namely a 15 ns and 100 kHz short pulse seeder, two fast axial flow pre- amplifiers with tube inner diameter 17 mm, and a main amplifier with tube inner diameter 30mm, RF pumped lasers. Figure 13 shows the overall configuration of the laser driver system, at 100 kHz repetition rate for the highest laser efficiency. The single-line oscillator is a small waveguide laser by a EO Q-switch at P(20) line.

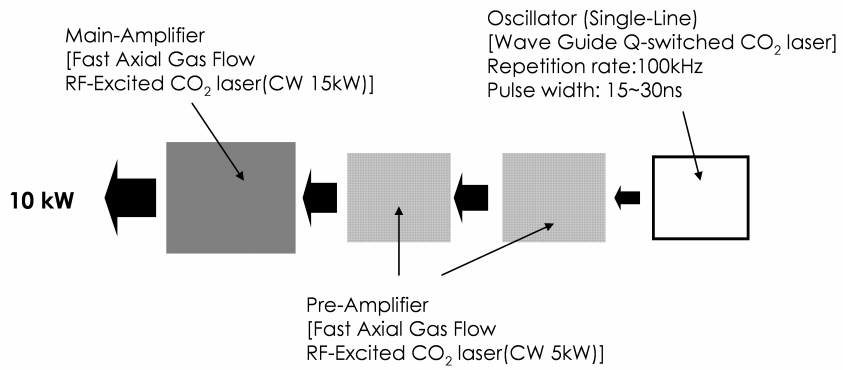

Figure.13 Configuration of the laser driver based on RF-pumped fast axial flow CO_2 laser

5.2 Characterization of low pressure CO_2 laser medium

The gain medium in CO_2 lasers is a CO_2:N_2:He gas mixture with pressures from 10 Torr to 10atmosphere depending on the excitation method. Low pressure system is employed in CW or fast repetition rate pulse system by RF excitation, and high pressure system is used for low repetition rate or single shot, high pulse energy applications by TEA discharge or electron beam excitations. The important relaxations are vibrational and rotational relaxations of the 00^01 band (τ_c and τ_r). These are typically 0.5 μsec and 1.5 ns in 100 Torr gas mixtures, respectively. The pulse train is composed of 10 ns pulses with 10 μsec time intervals. Thus the vibrational relaxation time is substantially longer then the pulse duration (τ_p), which implies that the amplification is only through the inversion built up in the main vibrational band during the pulse interval. The pulse duration is longer than the rotational relaxation time by less than an order of magnitude. Some contribution of the rotational relaxation must be considered in the pulse amplification. Considerable theoretical and experimental works have been performed for the development of TEA or multi atmospheric amplifiers designed for amplification of 1ns and down to 10 ps short pulses. The ratio of pulse width and relaxation time is $\tau_p/\tau_r \sim 10$ both in 1ns pulse amplification in 1 atmospheric gas mixture, and in 10 ns pulse amplification in 100 Torr gas mixture. It is thus useful to consider on the amplification study of 1ns pulses in a 1 atmosphere gas mixture, to estimate the behavior of the extraction efficiency of the 10 ns pulses in 100 Torr gas mixture. A numerical result is shown on a single pass amplifier of L=1 m long on the P(20) line in Fig.14 [8]. E_{in} is the input pulse fluence in mJ/cm^2, E_{out} is the output fluence, E_{max} is the maximum fluence given by $g_0 \cdot L \cdot E_s$, where $g_0$is the small signal gain coefficient in cm^{-1} , L is the gain length, and E_s is the saturation fluence in mJ/cm^2 . g_0 and E_s are functions of various parameters, namely gas pressure, mixture ratio, excitation density, pulse repetition rate, and input pulse spectrum. The Frantz-Nodvik equation describes the amplification in pulsed amplification.

$$E_{out} = E_s \cdot \ln[1 + \exp(g_0 \cdot L)[\exp(\frac{E_{in}}{E_s}) - 1]] \qquad (1)$$

More than 70 % of the available fluence is possible with $\tau_p / \tau_r = 11.6$ in the strong saturation amplification. Typical electrical efficiency of an axial flow CO_2 laser is around 20 % in CW oscillation, thus the expected maximum efficiency in a pulsed mode is more than 10 % after optimization.

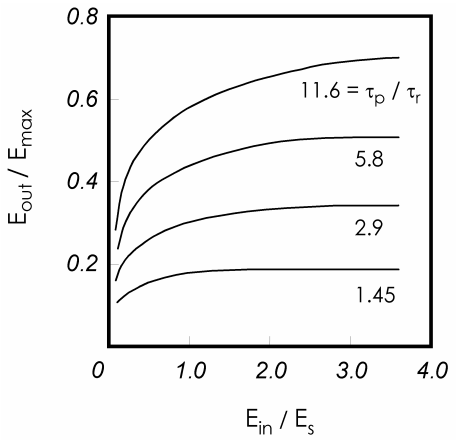

Figure.14 Calculated power extraction vs. pulse energy relations plotted for different values of the τ_p/τ_r parameter (τ_p = 1 ns, P(20)) [8].

5.3 Short pulse amplification of CO_2 laser MOPA system

Two cw 5kWlasers were used as pre-amplifiers and one cw 15kW laser was used as the main-amplifier as shown in Fig.13 for short pulse amplification. Special consideration is required to achieve efficient short pulse amplification in CW pumped gain modules. Parasitic oscillation inside the gain region, or optical coupling between two amplifier modules are typical problems in short pulse amplification in CW pumped gains. The gain region is not seeded by 10 ns

amplifying laser pulses during 10 μsec. Spontaneous emission could grow to a large signal to deplete the gain. An experiment was performed to confirm optical coupling without seeding. A power detector was set at the output window of the second and third amplifiers to measure a stray amplification. There was no power signal at full RF pumping of two preamplifiers and one main amplifier, which indicated no parasitic oscillation and optical coupling without seed laser pulse.

A compact, short pulse oscillator was installed as the seeder for the amplifiers. The laser was an EO Q-switched, 15 ns, single P(20) line, 100kHz, RF pumped waveguide CO_2 laser with 5 W output. Figure.13 shows the experimental arrangement of the 100 kHz laser system. 1kW was achieved by two pre-amplifier and a main amplifier amplification with seed power of 5 W. The short pulse amplification performance of the second pre-amplifier and the main amplifier have been estimated by amplification result using the Frantz-Nodvik equation. Figure.3 shows the short pulse MOPA system amplification performance by two pre-amplifiers and the main amplifier that uses estimated gain g_0 and saturation energy E_s of the pre-amplifier and main amplifier with 1 kW test result. The available output power is estimated from the present RF-excited MOPA system by use of a high power and short pulse Q-switched waveguide oscillator. A short pulse (pulse width in FWHM : < 30 ns), output power over 80 W and repetition rate of 100 kHz oscillator is installed into the system recently. A mode matching is very important for efficient power extraction, i.e. input beam profile has to match with the gain cross section of each amplifier. The seed laser beam diameter is expanded respectively in pre- and main amplifiers. The calculation result shows that 3 kW of the system output power is able to be achieved by a seeding power of 60 W in P(20) single mode amplification. Further power increase is envisioned by further optimization and a multi-line amplification scheme up to 10 kW.

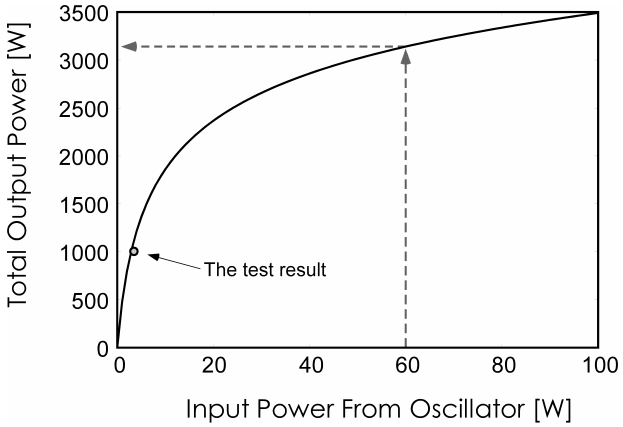

Figure.15 Output power estimation of the RF-excited MOPA system by use of a short pulse 60 W input power from an oscillator. The amplification test result with 1 kW output is plotted.

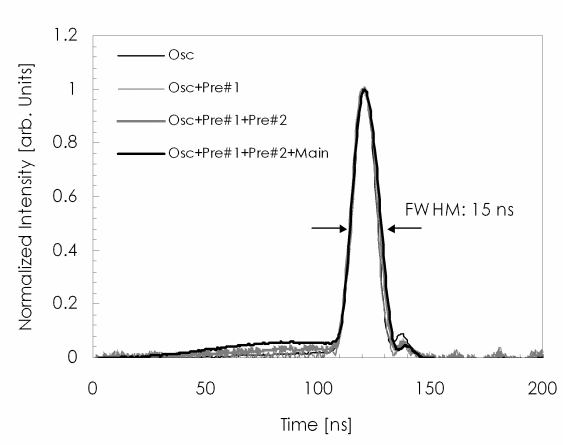

Figure.16 Input pulse shape of the EO Q-switched CO_2 oscillator and amplified laser pulseshapes after each stage

When there is a pedestal or tail in the input laser pulse, the pedestal and tail of the amplified laser pulse increases compared to the seed pulse. This means that the laser gain is used for amplification of the pedestal. The reduction of the pedestal is thus necessary for effective short pulse amplification. Pedestal of the seed laser pulse is able to be removed by use of CdTe Pockels Cell with a polarizer or saturable absorber gas cell which contains SF6 [9]. Figure.5 shows the time profile of laser pulses. In Fig. 16 "Osc" is a time profile of the EO Q-switched CO_2 laser that was used as an oscillator. "Osc+Pre#1", "Osc+Pre#1+Pre#2" and "Osc+Pre#1+Pre#2+Main" are amplification results with "first pre-amplifier", "first pre-amplifier + second pre-amplifier" and "first pre-amplifier + second pre-amplifier + main amplifier", respectively. A slight pedestal was accompanying before the main 15 ns pulse for 200 ns duration with 15 % energy of the main pulse when the oscillator pulse was amplified with the first pre-amplifier, the second pre-amplifier and the main amplifier. This means that there is a very slight pedestal on the oscillator pulse initially.

6. CONCLUSION

The feasibility of a pre-pulsed CO_2 laser driven Xe plasma EUV light source was experimentally evaluated. The EUV characteristics dependence on the delay time between the Nd:YAG pre-pulse and the CO_2 main laser pulse were measured including EUV conversion efficiency, plasma image, spectra of the EUV in-band and out-of-band region and fast ion energy distributions. The conversion efficiency was significantly increased by the pre-pulse laser irradiation. A maximum conversion efficiency of 0.6 % was obtained at a delay time of about 200 ns. The pre-pulse laser irradiation produced an ideal target density for CO_2 laser absorption at about 200 ns after pre-pulse irradiation. The peak energy of the fast ion energy distribution significantly decreased at delay times larger than about 200 ns. This result is promising for collector mirror lifetime extension by magnetic field mitigation. The feasibility of a CO_2 laser driven Xe plasma EUV light source and the effectiveness of pre-pulse laser irradiation were examined. The development of a short pulse, high average power CO_2 laser is reported on the general concept and its component characteristics. It is anticipated that the present matured CW CO_2 laser technology is well suited for a construction of a pulsed, high repetition rate laser system. A preliminary experiment demonstrated 1kW in 100kHz 15ns pulse amplification in a small signal gain region. Obtained laser parameters were used to estimate the obtainable power as to be 3kW with 60W seed in a saturation region in a single line amplification.The laser system is progressing on schedule to demonstrate a viable laser driver for Xenon or Tin droplet targets for 115W intermediate EUV power.

ACKNOWLEDGEMENTS

This work was supported by the New Energy and Industrial Technology Development Organization (NEDO), Japan.

REFERENCES

1. V. Banine, "Extreme ultraviolet sources for lithography applications", 3rd International EUVL Symposium, November 2004, Miyazaki, Japan, So01.
2. K. Nicklaus, M. Hoefer, H. D. Hoffmann, J. Luttmann, R. Wester, R. Poprawe, "MOPA with kW average power and multi MW peak power: experimental results, theoretical modeling and scaling limits" SPIE Photonics West 2006, San Jose 21-26 Jan.2006 [6100-33]
3. T.Ariga, H.Hoshino, T.Miura, A.Endo "High power and short pulse RF-excited CO_2 laser MOPA system for LPP EUV light source", SPIE Photonics West 2006, San Jose 21-26 Jan. 2006 [6101C-41]
4. H.Komori "EUV radiation characteristics of a CO_2 laser produced Xe plasma" submitted to Appl. Phys B
5. M.Nakano, A.Endo "Development of liquid Xenon droplet target for laser produced plasma EUV light source", Proceedings of Annual Meeting 2005, Japan Society of Fluid Mechanics , AM05-07-004
6. Lord Rayleigh, F.R.S "On the instability of jets" Proc.London mth Soc. 10(4)4-13, 1878
7. H. Komori, Y. Imai, G. Soumagne, T. Abe, T. Suganuma, A. Endo, "Magnetic field ion mitigation for EUV light sources", *Proc. SPIE*, **5751,** 859-866, 2005.
8. B. J. Feldman: Opt. Commun., 14, 13 (1975)
9. A. Endo, H. Hoshibo, T.Ariga and T.Miura: "Development of Short Pulse and High Power CO_2 Laser for EUV Lithograph", Proc. SPIE 5918, 149 (2005)